Development of a Numeric Predictor-Corrector Aerocapture Guidance for Direct Force Control

Daniel A. Matz* and Christopher J. Cerimele†
NASA Johnson Space Center, Houston, TX 77058

Direct force control, where the angle of attack and sideslip angle are modulated, has been proposed as an alternative to bank angle control for aero-assist maneuvers. This paper reimplements the current state-of-the-art aerocapture guidance for bank angle control, Fully Numeric Predictor-corrector Aerocapture Guidance (FNPAG), for direct force control. The optimal control theory underlying the structure of FNPAG is shown to not be applicable to the direct force control approach. Several solution structures for the longitudinal channel are compared by simulating dispersed three-degree-of-freedom trajectories for a reference mission consisting of a low lift-to-drag vehicle and a highly elliptical, 1-sol target orbit around Mars. The equations of motion for the lateral channel are derived, and a controller is designed to target a specified orbital plane. Finally, a Monte Carlo is used to demonstrate the performance of the new guidance.

I. Nomenclature

α = angle of attack
β = sideslip angle
γ = flight path angle
μ = gravitational parameter
ϕ = bank angle
σ = standard deviation
A = reference area
D = drag force
L = lift force
m = mass
$\overline{n}$ = unit vector normal to the targeted plane
p = out-of-plane position
r = radius
S = side force
v = velocity magnitude
$\underline{x}$ = position vector

II. Introduction

Bank angle modulation is a proven technique for controlling guided aero-assist maneuvers. The guidance algorithm decomposes the problem into a longitudinal and a lateral channel; however, the use of bank angle as the control parameter couples the two channels. The guidance prioritizes the longitudinal channel by allowing it to determine the magnitude of the bank angle command, and the lateral channel's only control is the sign of the command. A series of bank reversals, where the sign of the bank angle command is flipped, must be designed to drive the lateral error towards zero.

Direct force control (DFC) is being studied as an alternative to bank angle control [1]. Direct force control uses independent modulation of the angle of attack and sideslip angle. Assuming the bank angle is maintained at 0°, the longitudinal channel commands the angle of attack, and the lateral channel commands the sideslip angle. If the

*Aerospace Engineer, Flight Mechanics and Trajectory Design Branch, AIAA Senior Member
†Chief (retired), Flight Mechanics and Trajectory Design Branch, AIAA Senior Member

Table 1 Target Orbit.

Radius of Apoapsis	33 793 km
Radius of Periapsis	250 km
Inclination	90°
Longitude of Ascending Node	180°

Table 2 Initial Conditions.

Latitude	82°
Longitude	0°
Planetodetic Altitude	125 km
Inertial Velocity	6.2 km/s
Planetodetic Inertial Azimuth	180°

variations in the angle of attack and sideslip angle are relatively small, this effectively decouples the longitudinal and lateral channels.

Both of these control methods are applicable to various aero-assist maneuvers, but this paper will focus on aerocapture. The optimal bank angle profile for an aerocapture maneuver has been derived and used as the basis of the state-of-the-art aerocapture guidance Fully Numeric Predictor-corrector Aerocapture Guidance (FNPAG) [2]. In this paper, we will use FNPAG as a starting point and derive a new variant that commands angle of attack and sideslip angle. We'll refer to the original FNPAG algorithm as FNPAG Bank and our new variant as FNPAG DFC.

III. Simulation Configuration

The Flight Analysis and Simulation Tool (FAST) was used to generate dispersed, three-degree-of-freedom trajectories both to aid in the development of the new guidance algorithm and to evaluate its performance.

The guidance was assessed using a reference human Mars mission and vehicle configuration from the Entry, Descent, and Landing Architecture Study [3]. The vehicle is a 55 metric ton vehicle with a 70° sphere-cone aeroshell. The goal is to aerocapture into a highly elliptical, 1-sol orbit at Mars. The parameters for the target orbit are given in Table 1. The initial conditions are given in Table 2. The angle of attack and sideslip angle responses were emulated and the limits in Table 3 were enforced. In the given range of angles of attack and sideslip angles, the maximum L/D of the vehicle is 0.15. The atmosphere was modeled using Mars Global Reference Atmospheric Model (GRAM) 2010. When performing a Monte Carlo analysis, the dispersions in Table 4 were used. Note that no navigation or sensor errors were modeled.

After the aerocapture maneuver, the spacecraft must perform a series of burns to raise its periapsis, correct any remaining apoapsis error, and correct any remaining orbital plane error. These burns weren't simulated but were rather computed analytically using the conditions at atmospheric exit. We used the total ΔV of these maneuvers as a metric to assess the performance of the aerocapture maneuver.

IV. Guidance Development

FNPAG DFC is similar to FNPAG Bank in many respects. Each uses a numeric predictor-corrector for its longitudinal channel. The predictor in each guidance uses models of the vehicle aerodynamics and the planet's atmosphere and

Table 3 Direct force control angular limits.

	Angle Limit	Rate Limit	Accel Limit
Angle of Attack (α)	±9.51°	2.5 °/s	1.0 °/s^2
Sideslip Angle (β)	±5°	2.5 °/s	1.0 °/s^2

Table 4 Monte Carlo Dispersions.

Variable	Dispersion
GRAM Random Seed	uniform, 1–29999
GRAM Dust τ	uniform, 0.1–0.9
Mass	normal, $\sigma = 0.3333\,\%$
Aero Coefficients	uniform, $\pm 10\,\%$
Initial Longitude	normal, $\sigma = 0.083\,33°$
Initial Planetodetic Latitude	normal, $\sigma = 0.083\,33°$
Initial Planetocentric Inertial Flight Path Angle	normal, $\sigma = 0.033\,33°$
Initial Planetocentric Inertial Azimuth	normal, $\sigma = 0.083\,33°$
Initial Inertial Velocity	normal, $\sigma = 3.333\,\mathrm{m/s}$

gravity to propagate the aerocapture trajectory. Both guidances mitigate the effects of uncertainties in the vehicle aerodynamics and the planet's atmosphere by the use of estimators, which update the onboard models to match the sensed acceleration measured by the vehicle.

The differences between FNPAG Bank and FNPAG DFC are found in the details of the longitudinal and lateral channels. Assuming the vehicle maintains a bank angle of 0°, the longitudinal channel commands the angle of attack, and the lateral channel commands the sideslip angle. We further assume that the angle of attack and sideslip angle will remain small enough that any interaction between the channels can be neglected, such that the channels are decoupled. The details of the longitudinal and lateral channels will be discussed in the following sections.

A. Longitudinal Channel

The predictor requires an angle of attack profile when it integrates the trajectory. We desire a profile with only a single free parameter, so that the corrector has only a single variable for which to solve. In FNPAG Bank, the profile is based on the optimal bank angle profile [2]. We'll begin by reviewing the derivation of the optimal bank angle profile and then work through the selection of an angle of attack profile.

1. Review of Optimal Bank Angle Control for Aerocapture

Neglecting the planet rotation and assuming a spherical gravity model, the longitudinal equations of motion when using bank control are found as

$$\begin{aligned} \dot{r} &= v \sin\gamma \;, \\ \dot{v} &= -\frac{D}{m} - \frac{\mu \sin\gamma}{r^2} \;, \\ \dot{\gamma} &= \frac{1}{v}\left[\frac{L\cos\phi}{m} + \left(v^2 - \frac{\mu}{r}\right)\frac{\cos\gamma}{r}\right] \;. \end{aligned} \tag{1}$$

The bank angle is constrained by $\phi_{\min} < |\phi| < \phi_{\max}$.

The terminal condition is at apoapsis, where a constraint on the radius is specified, and the final time is free. The cost function is

$$J = \left(r - r\left(t_f\right)\right)^2 \;, \tag{2}$$

and the Hamiltonian is

$$H = \lambda_r v \sin\gamma + \lambda_v\left(-\frac{D}{m} - \frac{\mu\sin\gamma}{r^2}\right) + \lambda_\gamma\left[\frac{1}{v}\left(\frac{L\cos\phi}{m} + \left(v^2 - \frac{\mu}{r}\right)\frac{\cos\gamma}{r}\right)\right] \;. \tag{3}$$

Applying Pontryagin's Minimum Principle, we find

$$\begin{aligned} H\left(x^*, \phi^*, \lambda^*, t\right) &< H\left(x^*, \phi, \lambda^*, t\right) \;, \\ \frac{\lambda_\gamma^*}{v^*} L^* \cos\phi^* &< \frac{\lambda_\gamma^*}{v^*} L^* \cos\phi \;, \end{aligned} \tag{4}$$

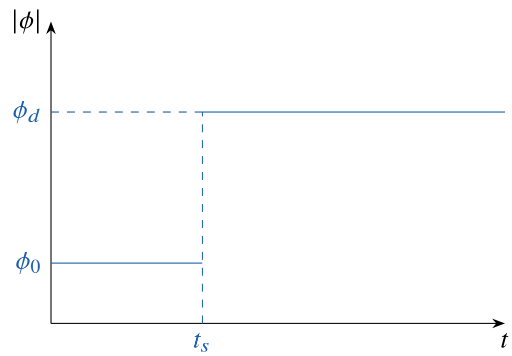

Fig. 1 Bank profile used in phase 1 of FNPAG.

where the $(\cdot)^*$ notation denotes optimal values. This yields three cases. If $\lambda_\gamma^* > 0$, we have

$$\begin{aligned} \cos\phi^* &< \cos\phi \, , \\ \phi^* &> \phi \, , \end{aligned} \tag{5}$$

which tells us that $\phi^* = \phi_{\max}$. If $\lambda_\gamma^* < 0$, we have

$$\begin{aligned} \cos\phi^* &> \cos\phi \, , \\ \phi^* &< \phi \, , \end{aligned} \tag{6}$$

which tells us that $\phi^* = \phi_{\min}$. The third case is when $\lambda_\gamma^* = 0$, which is a singular solution and can be shown to not be possible. Thus we see that the optimal solution for bank angle control has a bang-bang profile.

Based on this finding, FNPAG Bank was formulated as a two-phase numeric predictor-corrector. In the first phase, the predictor uses the bank angle profile shown in Figure 1, where ϕ_0 and ϕ_d are user-specified parameters, typically selected such that ϕ_0 is mostly lift up and ϕ_d is somewhat lift down. The corrector solves for the value of t_s such that the desired radius of apoapsis is achieved. Once the switching time is reached, the guidance enters phase 2, where the predictor uses a constant bank angle profile, and the corrector solves for the value of the bank angle such that the desired radius of apoapsis is achieved. For the lateral channel, FNPAG Bank predicts both the bank left and bank right solutions, compares them, and commands a user-specified number of bank reversals to produce a geometric reduction in the final orbital plane error [4].

2. Optimal Angle of Attack Control for Aerocapture

When using angle of attack and sideslip angle as the control variables, the longitudinal equations of motion are

$$\begin{aligned} \dot{r} &= v \sin\gamma \, , \\ \dot{v} &= -\frac{D(\alpha,\beta)}{m} - \frac{\mu \sin\gamma}{r^2} \, , \\ \dot{\gamma} &= \frac{1}{v}\left[\frac{L(\alpha,\beta)}{m} + \left(v^2 - \frac{\mu}{r}\right)\frac{\cos\gamma}{r}\right] \, . \end{aligned} \tag{7}$$

These equations are similar to those in Eq. (1), with the exception of the aerodynamic force terms. To simplify the problem and totally decouple the longitudinal and lateral channels, we assume the dependency of lift and drag on β is weak and neglect it. The angle of attack is constrained as $\alpha_{\min} < \alpha < \alpha_{\max}$.

If we try to apply optimal control theory as we did in the bank angle control case, we find the same cost function as in Eq. (2), but the Hamiltonian becomes

$$H = \lambda_r v \sin\gamma + \lambda_v\left(-\frac{D(\alpha)}{m} - \frac{\mu}{r^2}\sin\gamma\right) + \lambda_\gamma\left[\frac{1}{v}\left(\frac{L(\alpha)}{m} + \left(v^2 - \frac{\mu}{r}\right)\frac{\cos\gamma}{r}\right)\right] \, . \tag{8}$$

Applying Pontryagin's Minimum Principle, we find

$$\begin{gathered} H\left(x^*,\alpha^*,\lambda^*,t\right) < H\left(x^*,\alpha,\lambda^*,t\right) \ , \\ -\lambda_v^* D\left(\alpha^*\right) + \lambda_\gamma^* \frac{L\left(\alpha^*\right)}{v^*} < -\lambda_v^* D\left(\alpha\right) + \lambda_\gamma^* \frac{L\left(\alpha\right)}{v^*} \ . \end{gathered} \tag{9}$$

With two Lagrange multipliers, there are now several different cases to consider. For example, let's consider when $\lambda_v^* < 0$ and $\lambda_\gamma^* > 0$. In this case, the two terms have the same sign. Therefore, we desire a configuration that minimizes the drag force while producing the most negative vertical lift force. Intuitively, this leads us to choose $\alpha_{\max}$. Now consider when $\lambda_v^* > 0$ and $\lambda_\gamma^* > 0$. The two terms now have opposite signs, and there is no way to apply intuition to select a value of α. So, in general, the optimal angle of attack profile is not a bang-bang solution like we found for bank angle. Because both the lift and drag are functions of angle of attack, the optimal profile will at times require intermediate values of angle of attack.

3. Angle of Attack Profile Flyoff

While the optimal angle of attack profile remains unknown, we can still construct a predictor-corrector using a non-optimal angle of attack profile. We consider three candidate profiles. They are illustrated in Figure 2. Recall that for a blunt body an upward lift force is caused by a negative angle of attack.

The first candidate profile is a constant angle of attack, as shown in Figure 2a. The guidance is a single phase, and the predictor-corrector solves for the constant angle of attack that achieves the desired radius of apoapsis.

The second candidate profile varies the angle of attack linearly with specific energy, as shown in Figure 2b. The user specifies the value of the angle of attack at atmospheric exit, α_d. The guidance is again a single phase. The predictor-corrector solves for the current angle of attack such that the predicted trajectory, utilizing the linear profile, achieves the desired radius of apoapsis.

The third candidate uses a bang-bang profile, analogous to the approach used by FNPAG for bank control. The guidance has two phases. In the first phase, the predictor uses the profile in Figure 2c, with α_0 and α_d provided by the user. The corrector solves for t_s such that the desired radius of apoapsis is achieved. Once t_s is reached, the second phase of the guidance begins. In this phase, the predictor uses a constant angle of attack profile, and the corrector solves for the constant angle of attack such that the desired radius of apoapsis is achieved.

A dispersed flight path angle corridor scan was performed in order to compare the performance of the three candidate profiles. The dispersions in Table 4 were applied, except that the flight path angle was dispersed across the entire flight path angle corridor. The resulting total ΔV is shown in Figure 3. For our reference mission, the difference in performance between the three profiles is relatively small, especially on the shallow side of the flight path angle corridor where we would generally choose to fly.

Based on this comparison, we chose the bang-bang profile with a two-phase predictor-corrector. Its performance was generally the best of the three candidates. It isn't optimal, as we've shown, but it is analogous to the lift-up, lift-down profile used by FNPAG Bank.

B. Lateral Channel

When using bank angle control, the longitudinal and lateral channels are coupled. The lateral channel's only control is the sign on the bank angle. With direct force control, assuming the sideslip angle variation is small enough that its effect on lift and drag is negligible, we can decouple the longitudinal and lateral channels. The lateral channel can now produce a continuous sideslip angle command in order to drive the orbit into a specified plane.

We would like to construct a PD controller to command the sideslip angle according to

$$\beta = K_p p + K_d \dot{p} \ , \tag{10}$$

where p is the out of plane position, defined as $p = \underline{x} \cdot \overline{n}$, as shown in Figure 4. Selecting values for K_p and K_d directly is not intuitive. We would like to compute them based on vehicle parameters and performance characteristics.

As discussed above, the sideslip angle is limited to be within ±5°. For a sufficiently large value of p, we would want to use the full lateral control authority and saturate the sideslip angle command. By picking the saturation value of p, we can compute K_p as

$$K_p = \frac{\beta_{\max}}{p_{\text{saturation}}} \ . \tag{11}$$

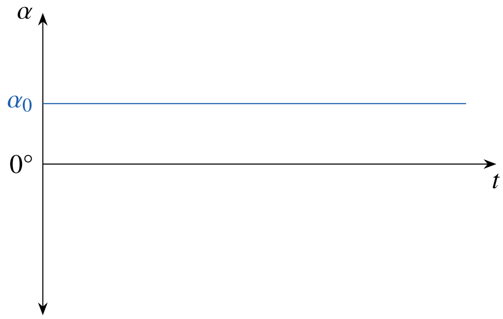

(a) The first candidate is constant.

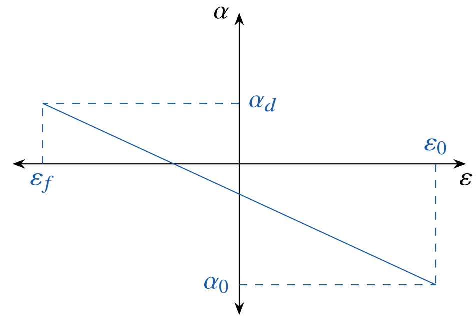

(b) The second candidate is linear with specific energy.

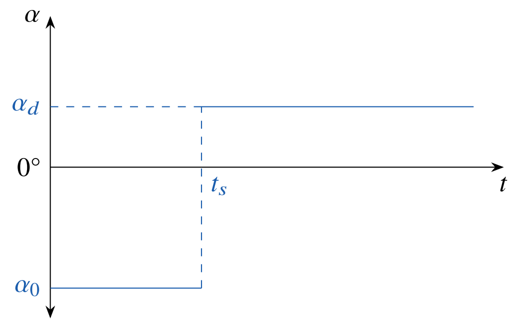

(c) The third candidate is bang-bang.

Fig. 2 Candidate angle of attack profiles.

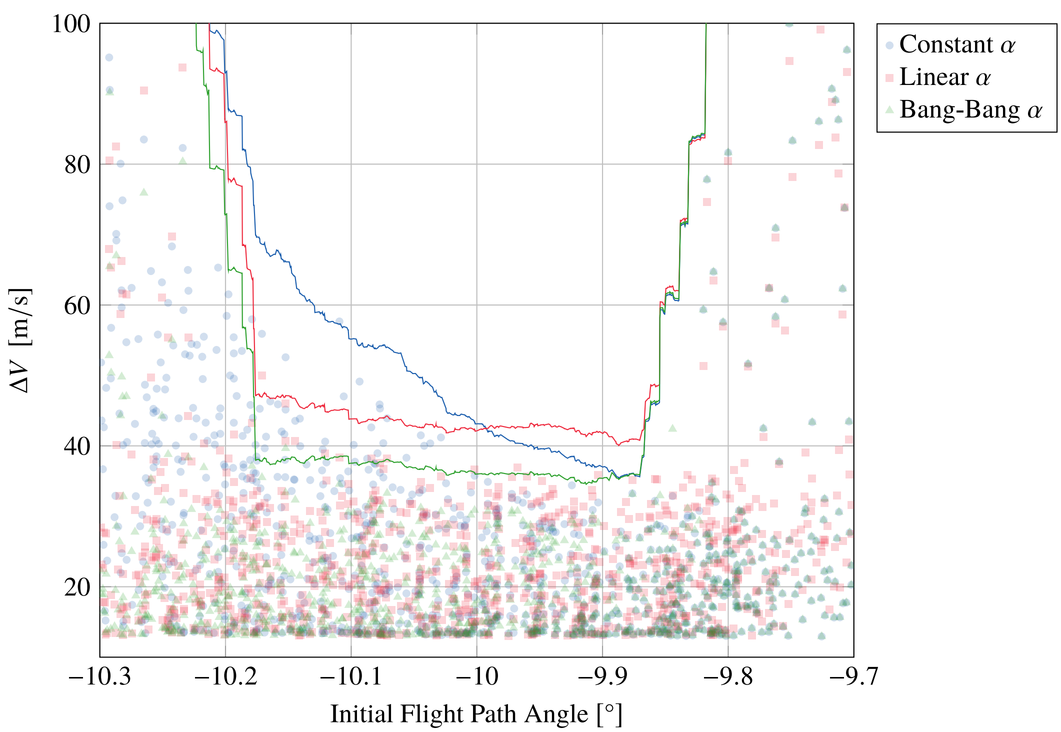

Fig. 3 Comparison of total ΔV for the candidate profiles across the flight path angle corridor. The dots are individual dispersed trajectories. The lines are the 3σ value of the dispersed cases for a local window of flight path angle.

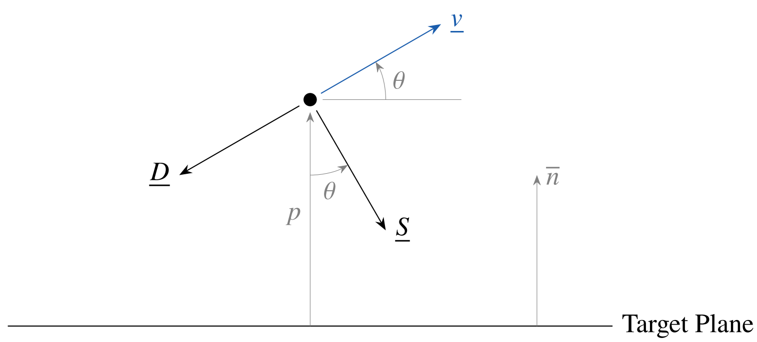

Fig. 4 The lateral motion of the spacecraft is defined relative to the target plane.

To compute K_d, we'll need to look again at the equations of motion. Beginning with Newton's second law, the equations of motion are

$$\begin{aligned} \underline{F} &= m\ddot{\underline{x}} \,, \\ \underline{D} + \underline{S} + \underline{L} - m\frac{\mu}{x^3}\underline{x} &= m\ddot{\underline{x}} \,. \end{aligned} \tag{12}$$

We are interested in the lateral motion of the spacecraft. Taking the dot product of each side of the equation with $\overline{n}$ yields

$$\underline{D}\cdot\overline{n} + \underline{S}\cdot\overline{n} + \underline{L}\cdot\overline{n} - m\frac{\mu}{x^3}\underline{x}\cdot\overline{n} = m\ddot{\underline{x}}\cdot\overline{n} \,. \tag{13}$$

The lift is orthogonal to $\overline{n}$, so that term vanishes. Assuming the angle θ shown in Figure 4 is small, then $\underline{S}\cdot\overline{n} = -S\cos\theta \approx -S$. The drag term always opposes velocity, such that we can rewrite it as $\underline{D} = -D\overline{v}$. We now have

$$-S - D\overline{v}\cdot\overline{n} - m\frac{\mu}{r^3}p = m\ddot{p} \,. \tag{14}$$

Since $\underline{v} = \dot{\underline{x}}$, we can rewrite

$$\overline{v}\cdot\overline{n} = \frac{\underline{v}\cdot\overline{n}}{v} = \frac{\dot{\underline{x}}\cdot\overline{n}}{v} = \frac{\dot{p}}{v} \,. \tag{15}$$

Substituting, we now have

$$-S - \frac{D}{v}\dot{p} - m\frac{\mu}{r^3}p = m\ddot{p} \,. \tag{16}$$

Next, we assume the drag coefficient is constant and that the side force coefficient is a linear function of β, such that

$$\begin{aligned} D &= qC_D A \,, \\ S &= qC_{S_\beta}\beta A \,. \end{aligned} \tag{17}$$

Substituting Eqs. (10) and (17) into Eq. (16) and rearranging terms yields

$$\ddot{p} + \left(\frac{qC_D A}{mv} + \frac{qC_{S_\beta}AK_d}{m}\right)\dot{p} + \left(\frac{qC_{S_\beta}AK_p}{m} + \frac{\mu}{r^3}\right)p = 0 \,. \tag{18}$$

Because we assumed θ is small, the total velocity magnitude, v, is essentially decoupled from $\dot{p}$, and so this is a second order system in p. Relating the terms of Eq. (18) to the standard form of a second order system, we find

$$\begin{aligned} \omega_n^2 &= \frac{qC_{S_\beta}AK_p}{m} + \frac{\mu}{r^3} \,, \\ 2\zeta\omega_n &= \frac{qC_D A}{mv} + \frac{qC_{S_\beta}AK_d}{m} \,. \end{aligned} \tag{19}$$

We determined K_p above and can therefore compute ω_n. Selecting a desired damping ratio, we can then compute

$$K_d = \frac{m}{qC_{S_\beta}A}\left(2\zeta\omega_n - \frac{qC_D A}{mv}\right) \,. \tag{20}$$

V. Results

For the initial condition, we selected a nominal flight path angle of $-9.95°$. For the longitudinal channel of the guidance, we selected $\alpha_0 = -9.51°$ and $\alpha_d = 2.5°$. We used a saturation out-of-plane position of 0.5 km and a damping ratio of 2.0 to compute K_p and K_d for the lateral channel. The overdamped lateral response was needed to compensate for the low limit on $\ddot{\beta}$, which can otherwise cause overshoot.

A Monte Carlo was run using the dispersions from Table 4. Time histories of one of the dispersed cases are shown in Figure 5. The two-phase nature of the angle of attack command is apparent. The angle of attack command trends back towards lift up as the vehicle exits the atmosphere, because the guidance is trying to fly out the remaining errors but is losing control authority as the dynamic pressure decreases. The out-of-plane position grows substantially at the beginning of the trajectory, before the dynamic pressure increases and the vehicle gains control authority. This results in a saturated sideslip angle command. The vehicle lacks sufficient lateral control authority, even when saturated, because of the tight limits placed on the sideslip angle. The lateral channel is able to fly out some of the errors, but the remaining error must be dealt with propulsively.

The results of the entire Monte Carlo are summarized in Figure 6. For the longitudinal channel, the cases achieve the targeted radius of apoapsis. For the lateral channel, the wedge angle, defined as the angle between the normal vectors of the current and targeted orbital planes, is still fairly large in many cases, because of the limited lateral control authority discussed above. Regardless, the total ΔV required to clean up the resulting orbit shows that both channels are performing well.

VI. Conclusion

We have developed a new guidance for aerocapture maneuvers using direct force control. The guidance is a variant of FNPAG, which was originally developed for bank angle control. The longitudinal channel uses a two-phase numeric predictor-corrector to command the angle of attack in order to achieve a desired radius of apoapsis. The lateral channel uses a PD controller to generate a continuous sideslip angle command to drive the trajectory into the desired orbital plane. The algorithm was applied to a low L/D reference vehicle and a reference mission of aerocapture into a highly elliptical, 1-sol orbit at Mars. Trajectory time history outputs show typical control responses. Monte Carlo results demonstrate the performance of the guidance when subjected to atmospheric, aerodynamic, and mass property dispersions.

References

[1] Dwyer-Cianciolo, A. M., and Powell, R. W., "Entry Descent and Landing Guidance and Control Approaches to Satisfy Mars Human Mission Landing Criteria," *AAS/AIAA Space Flight Mechanics Conference*, 2017.

[2] Lu, P., Cerimele, C. J., Tigges, M. A., and Matz, D. A., "Optimal Aerocapture Guidance," *Journal of Guidance, Control, and Dynamics*, Vol. 38, No. 4, 2015, pp. 553–565. doi:10.2514/1.g000713, URL `https://doi.org/10.2514/1.g000713`.

[3] Dwyer-Cianciolo, A. M., and Polsgrove, T., "Human Mars Entry, Descent, and Landing Architecture Study: Phase 2 Summary," *2018 AIAA SPACE and Astronautics Forum and Exposition*, 2018. doi:10.2514/6.2018-5190, URL `https://doi.org/10.2514/6.2018-5190`.

[4] Smith, K. M., "Predictive Lateral Logic for Numerical Entry Guidance Algorithms," *AAS/AIAA Space Flight Mechanics Meeting*, 2016. URL `https://ntrs.nasa.gov/search.jsp?R=20160001182`.

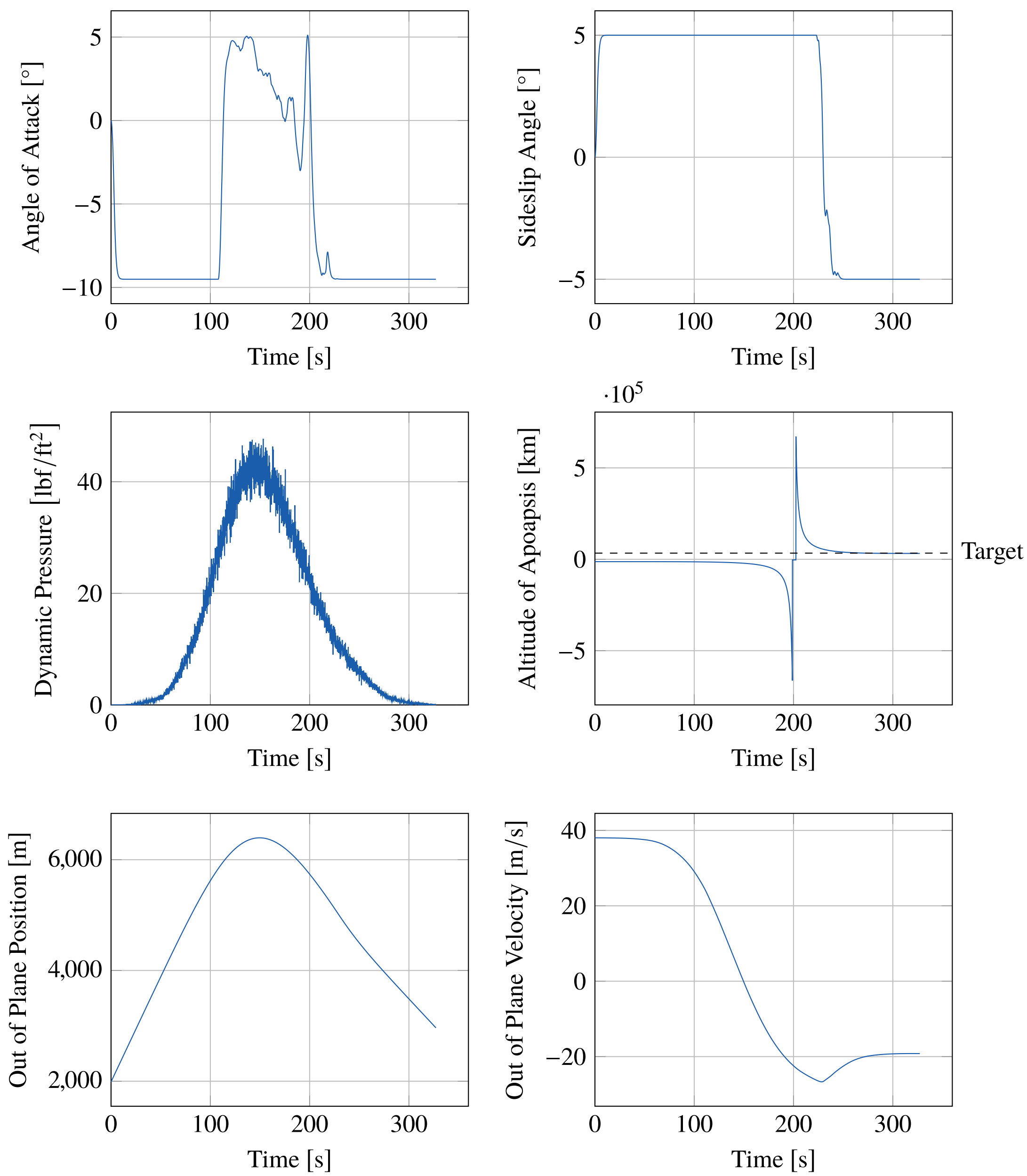

Fig. 5 The longitudinal channel uses a two-phase angle of attack profile to achieve a desired altitude of apoapsis. The lateral channel commands a continuous sideslip angle to null the out of plane position and velocity.

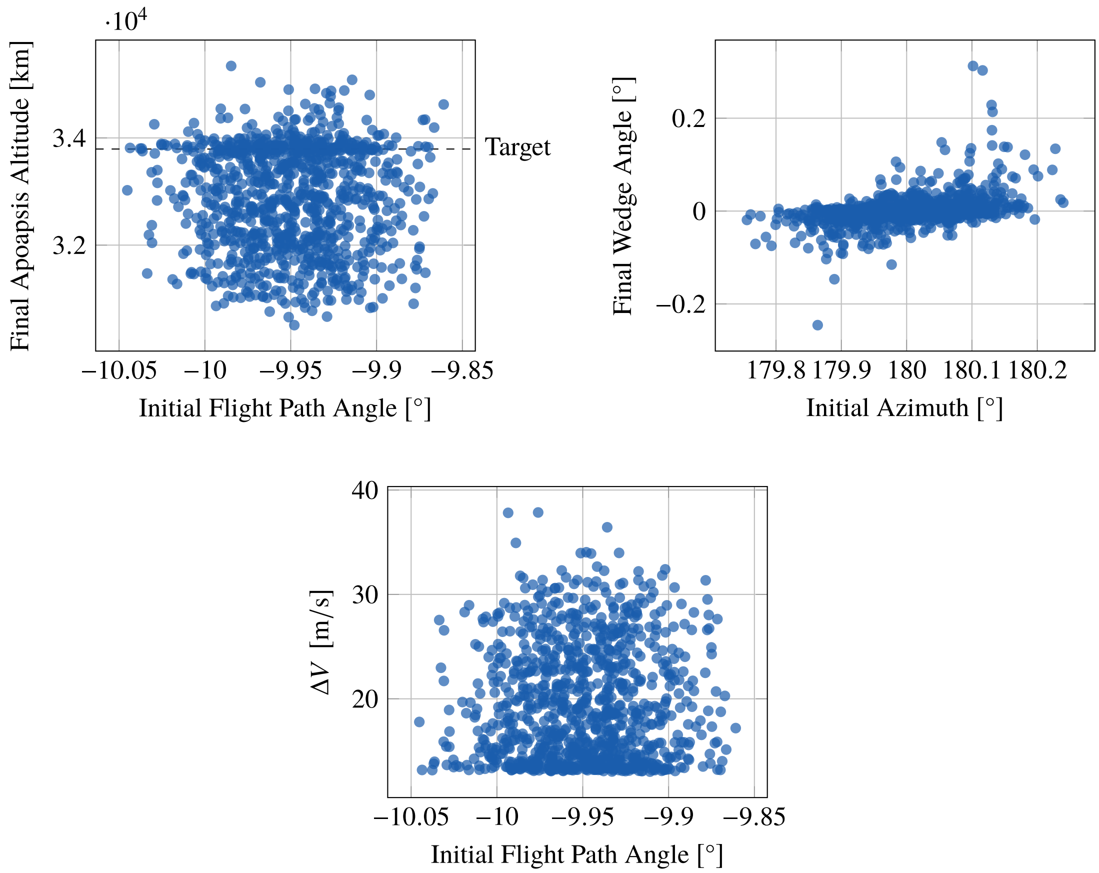

Fig. 6 Monte Carlo results.